

TRANSVERSE MULTI-BUNCH FEEDBACK DETECTOR ELECTRONICS USING DIRECT SAMPLING ANALOG-TO-DIGITAL CONVERTERS FOR THE SYNCHROTRON RADIATION SOURCE PETRA IV

S. Jablonski*, H.-T. Duhme, U. Mavrič, S. Pfeiffer, H. Schlarb
Deutsches Elektronen-Synchrotron, Hamburg, Germany

Abstract

PETRA IV, a new fourth generation synchrotron radiation source planned at DESY, will require a transverse multi-bunch feedback (T-MBFB) system to damp transverse instabilities and keep the beam emittance low. The critical part of the T-MBFB is a detector that must measure bunch-by-bunch, i.e. every 2 ns, position variations with the resolution not worse than 1 μm for the beam dynamic range of ± 1 mm. In this paper, we present the conceptual design of the T-MBFB detector from the beam position pickups to the direct sampling ADCs. We analyze noise sources limiting the detector resolution and present measurement results based on the evaluation modules.

INTRODUCTION

PETRA IV will operate in two modes, i.e. the brightness and timing mode. The requirements for the T-MBFB are summarized in Table 1. Due to short bunch spacing of 2 ns and low bunch charge of 0.4 nC in the brightness mode, it is more challenging to fulfill the resolution requirement of 1 μm in this mode than in the timing mode. Therefore, all performance calculations in this paper are done for the brightness mode. It is expected that in the timing mode the results are similar or better.

T-MBFB DETECTOR SCHEME

Figure 1 presents a simplified block diagram of the vertical T-MBFB detector electronics. The horizontal detector differs only in the connection of the stripline electrodes to the combiners in such a way that the detector is sensitive to horizontal bunch variations. Hence, it will not be discussed further in the text.

The stripline BPM is composed of four electrodes equally distributed around the beam pipe, i.e. every 90°, with a characteristic impedance Z_o of 50 Ω . For the vertical beam position measurement, electrical pulses from the upper and lower pick-ups are combined together, creating signals V_{AB} and V_{CD} , respectively. The signals are doubled in the pulse multiplier, and further, they are subtracted from each other in the bunch offset compensation. The difference signal ΔV is fed to the front-end electronics (DRTM-MBFB-FE) and the digitizer (DAMC-DS5014RT), which are implemented in the MicroTCA.4 form factor. The above mentioned hardware is described in more detail in the following sections.

* szymon.jablonski@desy.de

Table 1: PETRA IV design parameters in the brightness (B) and timing (T) mode and the requirements for the T-MBFB.

Design Parameter	Value
Energy E	6 GeV
Revolution freq. f_{rev}	130.12 kHz
Emittance ϵ_x/ϵ_y	< 20/4 pm rad (B) < 50/10 pm rad (T)
Total current I	200 mA (B), 80 mA (T)
Number of bunches	max. 3840 (B), 80 (T)
Bunch charge q_b	~0.4 nC (B), ~7.7 nC (T)
Bunch spacing T_{rep}	2 or 4 ns (B), 96 ns (T)
Bunch length σ_t	~45 ps (B), ~64 ps (T)
Betatron freq. f_x/f_y	23.4 kHz, 35.2 kHz
T-MBFB det. bandwidth	750 – 1250 MHz
Max. bunch offset r_{dc}	± 1 mm (from vacuum chamber center)
Max. betatron osc. amplitude r_{ac}	± 1 mm
T-MBFB det. resolution	< 1 μm (SNR > 60 dB)
T-MBFB damping time	< 40 turns (for $r_{ac} < 200 \mu\text{m}$)

MODEL OF THE PICKUPS AND ANALOG ELECTRONICS

Electron Bunch in the Vacuum Chamber Center

The frequency-domain transfer impedance of a stripline cylindrical electrode can be modelled as [1]:

$$Z(\omega) = j \frac{\alpha}{2\pi} Z_o \exp \left[-j\omega \left(\frac{L}{c_0} + \Delta t \right) \right] \frac{\sin(\omega\Delta t)}{\omega\Delta t} \sin \left(\omega \frac{L}{c_0} \right), \quad (1)$$

where c_0 is the speed of light in vacuum, L is the length of the electrode, R is the radius of the vacuum chamber, α is the electrode width in rad (geometric coverage factor), Δt is a time delay given by $\Delta t = R\alpha/c_0$. Assuming the electron bunch traveling in the middle of the vacuum chamber is a point charge in the transverse direction and has a Gaussian shape in the longitudinal direction with the rms bunch length of σ_t , the stripline coupler output voltage is

$$V(\omega) = Z(\omega)q_b \exp \left[\frac{-(\omega\sigma_t)^2}{2} \right], \quad (2)$$

where q_b is the bunch charge.

Figure 2 presents amplitude spectrum at the stripline coupler output for the brightness mode (3840 bunches, rep. rate

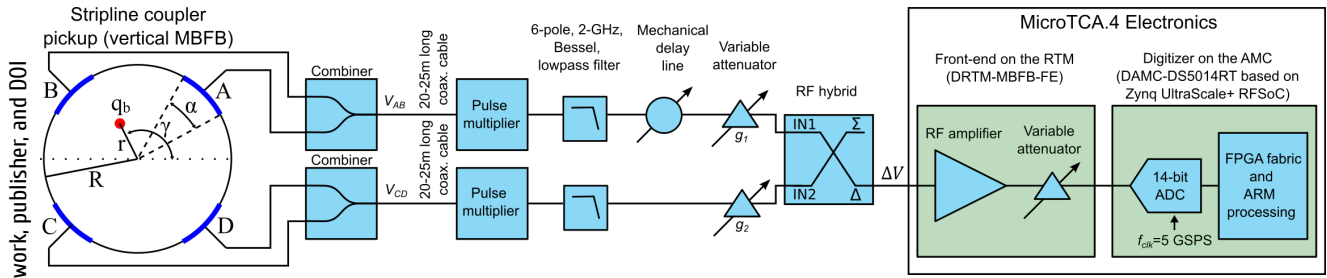


Figure 1: Simplified block diagram of the vertical T-MBFB detector electronics.

of 2 ns, $q_b=0.4$ nC, $\sigma_t=45$ ps) and for different electrode lengths L of 150 mm and 75 mm. The electrode length determines the optimal operating frequency of the receiver, which is around 500 MHz and 1 GHz, respectively. These frequencies correspond to the first and second harmonic of the multi-bunch spectrum with the bunch repetition rate of 2 ns. The vacuum chamber radius R is 17 mm and the electrode width α is 0.6 rad. The transfer function roll-off for the 150 mm-electrode is steeper and the magnitude decrease equals about 3 dB for the fastest multi-bunch mode at ± 250 MHz. Hence, we decided to use the shorter 75 mm-electrode, for which the magnitude decrease is only 1 dB.

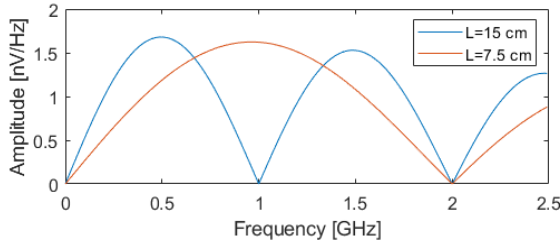


Figure 2: Amplitude spectrum at the stripline coupler output for the brightness mode (3840 bunches, rep. rate of 2 ns, $q_b=0.4$ nC, $\sigma_t=45$ ps) and for different electrode lengths L of 150 mm and 75 mm.

Instead of cylindrical electrodes, flat electrodes were selected as they are easier to be manufactured. However, the geometrical coverage factor is slightly different for both designs. Electromagnetic simulations [2] shown that the flat electrodes have lower sensitivity by a coefficient β of about 0.89, which will be further used to scale the signal amplitude.

Bunch Offset from the Vacuum Chamber Center

With different machine configurations, the electron bunch can be shifted by r from the centre of the vacuum chamber and rotated with respect to the electrode axis by an angle of γ (see Fig. 1). The output voltage $V(\omega)$ for different bunch positions is scaled by a coefficient $s(r, \gamma)$ given by [3]

$$s(r, \gamma) = 1 + \frac{4}{\alpha} \sum_{n=1}^{\infty} \frac{1}{n} \left(\frac{r}{R}\right)^n \cos(n\gamma) \sin\left(\frac{n\alpha}{2}\right). \quad (3)$$

Finally, the output voltage at each electrode is

$$V_x(\omega, r, \gamma_x) = \beta V(\omega) s(r, \gamma), \quad (4)$$

where the subscript x defines the electrode A, B, C or D. The electrode angles equal $\gamma_A = \gamma - \pi/4$, $\gamma_B = \gamma - 3\pi/4$, $\gamma_C = \gamma - 5\pi/4$, $\gamma_D = \gamma - 7\pi/4$. To make the detector sensitive only to vertical bunch oscillations, the upper and the lower electrode outputs must be combined together. The summed signals, using only the first order component of Eq. (3) (this simplification makes an estimation failure lower than 6% for small $r \leq 1$ mm), are given by

$$\begin{aligned} V_{AB}(\omega, r) &= V_A(\omega, r, \gamma_A) + V_B(\omega, r, \gamma_B) \\ &= \beta V(\omega) \left[2 + \frac{4\sqrt{2}}{\alpha} \left(\frac{r}{R}\right) \sin\left(\frac{\alpha}{2}\right) \right], \end{aligned} \quad (5)$$

$$\begin{aligned} V_{CD}(\omega, r) &= V_C(\omega, r, \gamma_C) + V_D(\omega, r, \gamma_D) \\ &= \beta V(\omega) \left[2 - \frac{4\sqrt{2}}{\alpha} \left(\frac{r}{R}\right) \sin\left(\frac{\alpha}{2}\right) \right] \end{aligned} \quad (6)$$

for γ in the range of $[0, \pi]$. Bunch offset from the vacuum chamber center r includes information about the vertical constant orbit shift r_{dc} and the vertical betatron oscillation amplitude r_{ac} , i.e. $r = r_{dc} + r_{ac}$.

Bunch Offset Compensation

For high detector resolution, the full-scale input range of an ADC should be used to sample only the betatron oscillation signal (amplitude modulation), which is about 22 dB weaker as the "carrier" signal. The carrier is suppressed by more than 30 dB by subtracting both signals V_{AB} and V_{CD} using an RF hybrid as shown in Fig. 1. Before subtraction, both signals are conditioned using variable attenuators g_1 and g_2 to get the same carrier amplitude. They are also filtered with a 6-pole, lowpass, 2 GHz bandwidth, Bessel filter having a transfer function $F(\omega)$. Due to linear phase response of the filter, it does not produce any ringing overlapping the next bunch. Assuming all electrical components are lossless, the vertical betatron oscillation voltage at the output of the bunch offset compensation equals

$$\begin{aligned} \Delta V(\omega) &= g_1 V_{AB}(\omega, r) - g_2 V_{CD}(\omega, r) \\ &= (g_1 + g_2) \beta V(\omega) F(\omega) \left[\frac{4\sqrt{2}}{\alpha} \left(\frac{r_{ac}}{R}\right) \sin\left(\frac{\alpha}{2}\right) \right]. \end{aligned} \quad (7)$$

SNR of the Analog Electronics

Integrating $\Delta V(\omega)$ within the MBFB detection range from 750 MHz to 1250 MHz for the maximum betatron oscillation amplitude of $r_{ac} = 1$ mm gives rms voltage of 0.25 V. Referring this voltage to thermal noise of 50 Ω load resistor gives SNR of 85 dB. However, the electrical components and 25-m long coaxial cables connecting the pickups and the detector electronics introduce insertion loss that degrades the SNR. The estimated loss is about 15 dB that reduces the SNR of the analog electronics to 70 dB, which is still 10 dB more than required for the T-MBFB. However, the resolution limiting component is the digitizer, which is discussed in the following section.

DIRECT SAMPLING DIGITIZER

Direct Sampling vs. Down-Conversion

MBFB systems are mainly based on two detection schemes, i.e. the direct sampling scheme as shown in Fig. 1 or the down-conversion scheme, which additionally involves an analog mixer in front of a digitizer to shift the detection band to baseband. In the past, the down-conversion scheme was preferred as ADCs did not have enough bandwidth for direct sampling of wideband RF pulses. In recent years, the ADC technology has moved forward - not only the input bandwidth and sampling rate have increased, but also ADC front-ends became better in terms of noise.

Noise floor of the down-conversion scheme is usually 3 dB lower than the direct sampling scheme (if using the same ADC for both cases). However, the direct sampling has a few advantages over the down-conversion:

- The down-conversion requires a more complex hardware including the local oscillator (LO).
- The baseband detectors are more susceptible to electromagnetic interference (EMI), e.g. due to switched-mode power supplies.
- Up-conversion of $1/f$ noise of the ADC front-end is reduced in the direct sampling suppressed carrier detector [4] (carrier suppression is implemented in the bunch offset compensation module). In contrary, the baseband detector resolution degrades due to $1/f$ noise of the ADC.
- Designing of the front-end electronics with flat magnitude and linear phase is more difficult for the baseband detector ([23.4 kHz, 250 MHz] spans over 4.03 decades) than for the direct sampling detector ([750 MHz, 1250 MHz] spans only over 0.22 decades). Moreover, the DC coupling of the baseband detector requires additional electronics for the common-mode voltage adjustment.

Zynq UltraScale+ RFSoc

Taking into account the pros and cons of both detector schemes, the direct sampling has been selected using the Zynq UltraScale+ RFSoc ADC. It has 14-bit resolution, sampling rate of 5 GSPS and an input bandwidth of 6 GHz. This module includes also FPGA and processing system

that allows for flexible data processing like I/Q digital down-conversion, calculation of the bunch-by-bunch oscillation amplitudes and the transverse MBFB implementation.

Digitizer Noise and Interleaving Spurs

The betatron oscillation signal converted to digital can be written as [5]

$$\Delta V_k = [n_k + \Delta V(kT_s - x_k)](1 - r_k) + n_q, \quad (8)$$

where k is the sample number, T_s is the sampling period, n_k is the additive noise of the ADC input stage, x_k is the combined timing jitter caused by aperture jitter (time fluctuations in the ADC sample and hold) and by clock timing jitter, r_k is the voltage reference noise, n_q is the quantization noise (white, uniformly distributed with zero-mean). Noise sources n_k , x_k , r_k and n_q are independent random processes.

Timing jitter x_k has a negligible impact for the amplitude measurements. Quantization noise PSD can be estimated by

$$S_{n_q}(f) = -20 \log(2^m) - 10 \log(f_s/2) \approx -178 [\text{dBFS}/\text{Hz}], \quad (9)$$

where m is the number of bits (14) and of f_s is the sampling rate (5 GSPS), which is also a negligibly small number. The voltage reference noise r_k is usually considerably lower than the input stage additive amplitude noise [5], which was measured to be -155 dBc/Hz at 1 GHz. The integrated amplitude noise within the detector range gives the SNR of 67 dB. However, the single pulse, corresponding to one bunch, occupies about a half of the possible measurement 2-ns time window that reduces the SNR by about 3 dB down to 64 dB — this is shown in more detail in the next section.

Each of the ADCs in the Zynq UltraScale+ RFSoc is built on multiple sub-ADCs in an interleaving architecture. The interleaving process requires that a calibration algorithm to be carried out, described in detail in Ref. [6]. Because of the suppressed-carrier operation of the T-MBFB, the ADCs can only be calibrated in the machine start-up. Later the calibration coefficients are frozen. The long-term behaviour of the ADCs needs to be studied in detail, but we do not expect any detrimental effects, because the system is located in a temperature stabilized environment.

Even if the calibration procedure is carried out, there are some residual interleaving spurs. Since the gain and time skew spurs depend on the input signal level, they are very low for no-carrier operation. The DC offset spurs at $n f_s/8$ ($n = 1 \dots 8$) are below 80 dB and the sampling frequency f_s is so selected that the spurs do not overlap with the coupled-bunch oscillation modes.

SNR Improvement - ADC Parallelization and Pulse Multiplication

The basic detector structure provides the detector SNR of 64 dB, which is a 4-dB safety margin to the requirements. However, the SNR can be further improved by two hardware extensions, i.e. ADC parallelization and pulse multiplication.

Content from this work may be used under the terms of the CC-BY-4.0 licence © 2023. Any distribution of this work must maintain attribution to the author(s), title of the work, publisher, and DOI

The single RFSoc module includes eight ADCs. Four ADCs can be used for the T-MBFB detector and the rest are planned to be used for different diagnostics like the measurement of bunch-by-bunch phase or absolute bunch position in the vacuum chamber. The noise floor improvement factor is a square root of the number of parallel ADC channels, which is 6 dB for four ADCs. The parallelization not only improves the detector resolution, but it also provides redundancy in case of hardware failures.

The pulse multiplier improves the resolution by 3 dB, which was presented in our previous publication [7].

DIGITIZER PERFORMANCE EVALUATION AT PETRA III

The digitizer performance was evaluated at PETRA III using the sum signal from four stripline electrodes. The sum signal amplitude depends only on the bunch charge, it does not change with the transverse bunch oscillations. Since, the bunch charge is relatively stable (life time is about 1.5 h, the short-term pulse amplitude variations are dominated by residual amplitude noise of the ADC. Figure 3 presents the pulse signal converted to digital with the sampling clock of about 5 GSPS generated by the RFSoc internal PLL and synchronized to the machine main oscillator. In the digital domain, the RF pulse is IQ down-converted to baseband, lowpass filtered and decimated by 10. Using IQ values, the bunch-by-bunch and turn-by-turn amplitudes are calculated. In the next step, the SNR is computed for each bunch in the bunch train based on 132 revolutions, the SNR values are presented in Fig. 4. The averaged SNR equals 66 dB, which is only 1 dB worse than was estimated for 2-ns long pulse using the laboratory setup. In the future PETRA IV, the single pulse will be twice shorter (as written in the previous sections), therefore the SNR will decrease down to 63 dB.

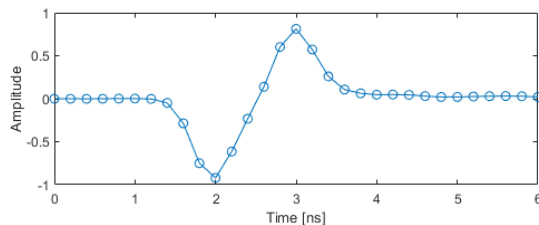


Figure 3: Digitized bunch pulse at PETRA III with the sampling rate of 5 GSPS.

CONCLUSION

In this paper, we presented the structure of the T-MBFB detector for PETRA IV. The detector resolution, specified

by SNR, was analyzed separately for the analog electronics and the digitizer. The analog electronics was analytically modelled to have SNR better than 70 dB. The digitizer was experimentally tested both in the laboratory conditions and at PETRA III. The analysis shows that the dominant noise source is the digitizer front-end noise, which limits the detector resolution to 63 dB for the PETRA IV system. This

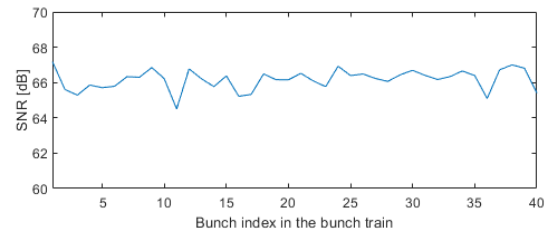


Figure 4: SNR of the RFSoc based T-MBFB detector evaluated at PETRA III in the timing mode with 40 bunches.

fulfills the project requirements, however, if needed in the future, the SNR can be improved by the ADC parallelization and pulse multiplication to more than 70 dB.

REFERENCES

- [1] M. Wendt, “BPM Systems: A brief Introduction to Beam Position Monitoring”, 2020. doi:10.48550/arXiv.2005.14081
- [2] S. Stokov, “Stripline monitor simulation. S-parameters, Signal strength and quality”, Internal Report, Aug. 2022.
- [3] R. E. Shafer, “Beam position monitoring”, in *AIP Conf. Proc.*, vol. 212, pp. 26–58, 1990. doi:10.1063/1.39710
- [4] E. Rubiola and V. Giordano, “Advanced interferometric phase and amplitude noise measurements”, in *Rev. Sci. Instrum.*, vol. 73, no. 6, pp. 2445–2457, Jun. 2002. doi:10.1063/1.1480458
- [5] A. C. Cárdenas-Olaya, E. Rubiola, *et al.*, “Noise characterization of analog to digital converters for amplitude and phase noise measurements”, in *Rev. Sci. Instrum.*, vol. 88, no. 6, pp. 065108, Jun. 2017. doi:10.1063/1.4984948
- [6] Zynq UltraScale+ RFSoc RF Data Converter v2.6 Gen 1/2/3/DFE LogiCORE IP Product Guide (PG269), <https://docs.xilinx.com/r/en-US/pg269-rf-data-converter/RF-ADC-Calibration-Mechanism>
- [7] S. Jabłoński *et al.*, “Conceptual Design of the Transverse Multi-Bunch Feedback for the Synchrotron Radiation Source PETRA IV”, in *Proc. IBIC’22*, Kraków, Poland, Sep. 2022, pp. 488–491. doi:10.18429/JACoW-IBIC2022-WEP36